CrossMark

Nanophase Ru–RuO$_2$ composites decorated on wrinkled Nb-doped TiO$_2$ nanofibers for electrochemical capacitors

Hye Lan An · Yu-Jin Lee · Hyo-Jin Ahn

Abstract Here, we studied nanophase Ru–RuO$_2$ composites decorated on wrinkled Nb-doped TiO$_2$ (NTO) nanofiber (NF) supports for electrochemical capacitors. These compositions were synthesized by an electrospinning method and an impregnation method. To investigate the electrochemical performance of electrochemical capacitors, 20 wt% nanophase Ru–RuO$_2$ composites were decorated on wrinkled NTO NF supports doped with three different amounts of Nb. The structural, morphological, chemical, and electrochemical properties of the composite nanophases were investigated using field emission scanning electron microscopy, transmission electron microscopy, Brunauer–Emmet–Teller analysis, X-ray diffraction, X-ray photoelectron spectroscopy, and cyclic voltammograms (CVs). The CV results indicated that the nanophase Ru–RuO$_2$ composites decorated on the wrinkled NTO NFs possessed superior capacitance ($\sim$496.3 F/g at 5 mV/s) and good high-rate capacitance because of the synergistic effect of the increased specific surface area of the wrinkled NTO NF supports and the presence of the nanophase Ru–RuO$_2$ composites.

Keywords Electrochemical capacitors · Nanophase Ru–RuO$_2$ composites · Nb-doped TiO$_2$ nanofibers · Electrospinning method · Impregnation method

HyeLan An and Yu-Jin Lee have contributed equally to this article.

H. L. An · Y.-J. Lee · H.-J. Ahn (✉)
Department of Materials Science and Engineering, Seoul National University of Science and Technology, Seoul 139-743, Korea
e-mail: hjahn@seoultech.ac.kr

🕿 Springer

Introduction

Energy storage devices such as electrochemical capacitors and batteries are currently of great interest because of the rapid development of electronic devices such as electric vehicles, flashlights, laptops, and mobile phones [1, 2]. Compared to other energy storage devices, electrochemical capacitors have advantages such as high power density, high rate capability, and long cycle life [3, 4]. Furthermore, electrochemical capacitors, which store electrical energy in an electrical double-layer, operate via two different storage mechanisms. One mechanism is that of electrical double-layer capacitors (EDLCs) operating via a non-faradaic process. EDLCs use carbon-based materials such as graphene, carbon nanofibers (CNFs), carbon nanotubes (CNTs), and activated carbon. The other mechanism is that of metal chalcogenides and transition metal oxide (i.e., RuO_2, Co_3O_4, and MnO_2) pseudocapacitors operating via a faradaic process [5, 6]. Among the various materials used for pseudocapacitors, RuO_2 electrodes are the most widely used because of their high energy density (10.7 Wh/kg) and high specific capacitance (768 F/g). However, in spite of these advantages, the increasing high cost of RuO_2 electrodes has been the biggest barrier for their industrialization. To solve these problems, researchers have investigated the use of (1) composite structures, (2) porous structures, and (3) the use of supports [7]. Of these strategies, the use of supports such as oxide-, carbon-, and polymer-based supports has been actively studied for use in electrochemical capacitors [8–10]. In particular, for the case of oxide-based supports, Nb-doped TiO_2 (NTO) nanofibers (NFs), which have good electrical and optical properties, have been actively used in energy storage devices (i.e., fuel cells and Li-ion batteries) and transparent conductive oxides (TCOs) [11–13]. For example, Gojkovic′ et al. [11] reported an NTO support prepared by an acid-catalyzed sol–gel method for use in fuel cells. The activities of methanol oxidation for Pt/NTO and Pt–Ru/NTO, which are synthesized by sol–gel and reduction methods, exhibited values similar to those of conventional Pt/XC-72 and Pt–Ru/XC-72. Wang et al. [12] synthesized mesoporous NTO by a polymer-assisted sol–gel process and then used it as the positive electrodes for Li-ion batteries. When the NTO electrode was used as a cathode, it showed a highly stable capacity ($\sim$160 mAh/g) after 100 cycles. Gillispie et al. [13] reported NTO transparent conductive films prepared using radio frequency magnetron sputtering. NTO films deposited at 370 °C showed superior performance such as a conductivity of $\sim$60 S/m, a carrier concentration of 1.5×10^{21} cm^{-3}, and a motility of less than 1 cm^2/Vs. Furthermore, our group synthesized wrinkled NTO NFs by electrospinning and investigated their formation mechanism using different mole ratios of the Nb precursor to the Ti precursor [14]. We found that, among various parameters (i.e., particle size, composite ratio, doping materials, and porosity) for high-performance electrochemical capacitors, modifying the morphology of the electrodes is one of the key factors for improving their performance. From this standpoint, a study on electrochemical capacitors fabricated using wrinkled NTO NF supports, which has not been reported until now, is a very important issue.

In this work, we synthesized 20 wt% nanophase Ru–RuO_2 composites and decorated them on wrinkled NTO supports by electrospinning and impregnation

methods. We also demonstrate their electrochemical performance for electrochemical capacitors.

Materials and methods

Materials

First, 20 wt% nanophase Ru–RuO$_2$ composites decorated on NTO NF supports were synthesized by electrospinning and impregnation methods. *N,N*-dimethylformamide (DMF), poly(vinylpyrrolidone) (PVP, M_w = 1,300,000 g/mol), acetic acid (99.7 %), titanium (IV) isopropoxide (97 %), niobium (V) ethoxide (99.95 % metals basis), ruthenium (III) chloride hydrate (RuCl$_3$·xH$_2$O), and sodium borohydride (NaBH$_4$, 98 %) were purchased from Sigma-Aldrich.

Synthesis of wrinkled NTO NF supports

Niobium (V) ethoxide is added to the precursor solution consisting of titanium (IV) isopropoxide as a precursor, PVP as a stabilizer, and acetic acid as a dispersant of the solution dissolved in DMF. To synthesize three different types of wrinkled NTO NF supports, we controlled the mole ratios of the Nb precursor to the Ti precursor to 0, 0.23, and 0.59 M [14]. The prepared precursor solutions were added to a syringe equipped with 23-gauge needle. The feeding rate, distance between the needle tip and the collector (Al foil), and applied voltage were fixed at ∼0.04 mL/h, ∼20 cm, and 14.5 kV, respectively. All the resultant samples were calcined at 500 °C for 5 h in atmosphere. It was observed that the greater the amount of Nb precursor used, the better formed were the wrinkled NTO NFs.

Synthesis of nanophase Ru–RuO$_2$ composites decorated on NTO NF supports

In order to use them as electrodes in electrochemical capacitors, the nanophase Ru–RuO$_2$ composites were decorated on three different types of NTO NF supports by an impregnation method. That is, after dispersion of the as-prepared NTO NF supports in de-ionized (DI) water, we decorated them by adding 0.56 mM RuCl$_3$·xH$_2$O. The resulting solutions were continually mixed by alternating stirring and sonication for 1 h. For the impregnation process using the Ru precursor, we added NaBH$_4$ as a reducing agent to the above-mentioned solution. Finally, the resultant samples were washed several times in DI water. The resultant samples were dried at 100 °C for 3 h in a convection oven. As a result, nanophase Ru–RuO$_2$ composites decorating single TiO$_2$ NFs, 0.23 M Nb-doped TiO$_2$ NFs, and 0.59 M Nb-doped TiO$_2$ NFs were successfully synthesized. The samples are referred to here as sample A, sample B, and sample C, respectively.

Structural and elemental characterization

Analysis of the morphology and structure of the samples was performed using field emission scanning electron microscopy (FESEM; Hitachi S-4700) and multi-functional transmission electron microscopy (MULTI/TEM; Tecnai G^2; KBSI Gwangju Center). To measure the surface areas of the NF supports, the Brunauer–Emmet–Teller (BET; Micromeritics ASAP2010) method by N_2 adsorption at 77 K was used. The crystal structure and chemical bonding states of the samples were characterized by X-ray diffraction (XRD; Rigaku Rint 2500 equipped with a Cu K_α radiation source) and X-ray photoelectron spectroscopy (XPS; ESCALAB 250 equipped with an Al K_α X-ray source).

Measurement of capacitance

Electrochemical performance was measured using a potentiostat/galvanostat (PGST302N; Eco Chemie, The Netherlands) with a conventional three-electrode system: a working electrode, a reference electrode, and a counter electrode. The working electrode was fabricated by inks consisting of the as-prepared samples, acetylene black, and a polyvinylidene fluoride (PVDF) binder, which was controlled to have a mass ratio of 7:2:1 in N-methyl-2-pyrrolidinone (NMP). The inks (3 μL) were loaded on the glassy carbon working electrode (55 mm length, 6.35 mm diameter, 7.06 mm^2 surface area; CH Instruments) and dried at 70 °C for 0.5 h. The mass of active materials loaded on the glassy carbon electrode for all samples was fixed at 0.257 mg/cm^2. Ag/AgCl (sat. KCl) and Pt wire were used as the reference and counter electrodes, respectively. The electrolyte used was a 0.5 M H_2SO_4 solution. Cyclic voltammograms (CVs) were characterized using a potentiostat/galvanostat at scan rates of 5, 10, 30, 50, and 100 mV/s in a potential range 0.0–1.0 V versus Ag/AgCl (sat. KCl). To obtain the capacitance of the electrodes, we used the following equation [9, 15]:

$$C = (q_a + q_c)/(2m \times \Delta V)$$

where q_a, q_c, m, and ΔV are the charge of the anodic region, charge of the cathodic region, mass of active materials (g), and potential range of the CVs (V), respectively. In addition, the gravimetric capacitance (C_g, F/g) of all the samples was normalized by considering the mass of the Ru electrode.

Results and discussion

Figure 1a–c shows the FESEM images obtained from samples A, B, and C. The morphological properties of the samples indicate cylindrical NFs for sample A, wrinkled NFs for sample B, and wrinkled NFs for sample C. We think that the formation mechanism of samples B and C having the wrinkled morphology is related to two reasons: one is owing to the agglomeration of Ti precursors and Nb precursors linked by PVP in the as-spun NFs, the other is owing to the buckling effect of a cylindrical polymer shell, arising from removal of solvent during the

electrospinning process [16]. The respective diameters of samples A, B, and C were in the range of $\sim$91–151, $\sim$100–152, and $\sim$128–204 nm, respectively. In particular, the specific surface area of the samples, which was obtained by the BET measurements, increased gradually as the amount of Nb doped in the TiO$_2$ NFs increased: 33.0 m^2/g for sample A, 87.2 m^2/g for sample B, and 128.4 m^2/g for sample C. The enhanced specific surface area of the samples is strongly related to the improved performance of the electrochemical capacitors. In addition, the samples exhibited slightly rough surface morphology because of the nanophase Ru–RuO$_2$ composites. To further examine the morphological and structural properties of the samples, TEM measurements were performed.

Figure 2 shows the low-resolution TEM images (a–c) and the enlarged high-resolution TEM images (d–f) of samples A, B, and C, respectively. All the samples exhibited relatively dark blobs on the NFs, indicating nanophase Ru–RuO$_2$ composites having $\sim$2.0–3.4 nm in size. In particular, the wrinkled structures of samples B and C show uniform distribution of the nanophase Ru–RuO$_2$ composites as compared to the cylindrical structure of sample A owing to the high surface area of the wrinkled NF structures. This improved distribution of the nanophase Ru–RuO$_2$ composites plays an important role in improving the efficiency of electrochemical capacitors. It is well known that one of the biggest problems in using one-dimensional nanostructures in energy storage devices such as electrochemical capacitors is their relatively low specific surface area as compared to zero-dimensional nanostructures. Thus, the improved characteristics of the wrinkled NTO NF supports will make it possible to apply to them to high-performance electrochemical capacitors fabricated using one-dimensional nanostructures.

Figure 3 shows the XRD plots obtained from samples A, B, and C. The reference bulk reflections of pure RuO$_2$, pure Ru, anatase TiO$_2$, and rutile TiO$_2$ phases are shown at the bottom of Fig. 3. The main diffraction peaks of sample A are observed at 25.3°, 37.8°, and 48.0°, corresponding to the (101), (004), and (200) planes, respectively, of anatase TiO$_2$ phases [JCPDS card No. 841286], and at 27.9°, 36.4°, 41.7°, and 55.1°, corresponding to the (110), (101), (111), and (211) planes, respectively, of rutile TiO$_2$ phases [JCPDS card No. 870920]. This result implies that sample A is composed of anatase TiO$_2$ phases with a tetragonal structure (space group I4$_1$/amd [141]) and rutile TiO$_2$ phases with a body-centred tetragonal structure (space group P4$_2$/mnm [136]). As the amount of Nb doping for samples B and C increased from 0.23 to 0.59 M, the TiO$_2$ phases transformed from an anatase structure to a rutile structure. With this structural transformation, the NTO NF supports changed from the cylindrical morphology to the wrinkled morphology, which caused an increase in the specific surface area of the NTO NF supports. Furthermore, for the case of nanophase Ru–RuO$_2$ composites, no diffraction peaks are observed. It seems that the diffraction peaks for the nanophase Ru–RuO$_2$ composites are buried in the crystalline NTO phases, such that their high intensity peaks are masked, because of the small size and small amount of the nanophase Ru–RuO$_2$ composites. To further elucidate the chemical composition and chemical bonding states, we carried out XPS measurements.

Figure 4 shows the XPS spectra obtained from sample C. The Nb 3$d_{5/2}$ and Nb 3$d_{3/2}$ spectral peaks shown in Fig. 4a are observed at $\sim$206.9 and $\sim$209.6 eV,
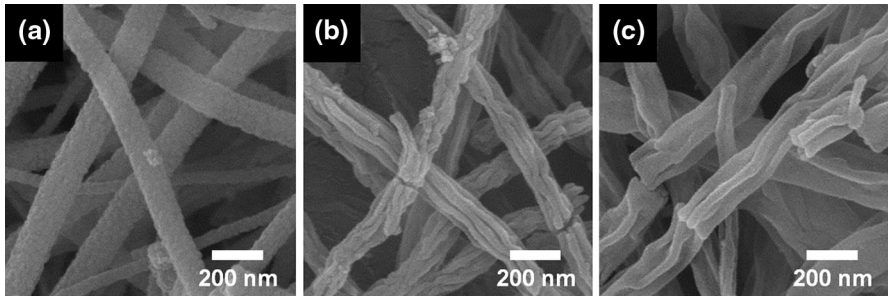
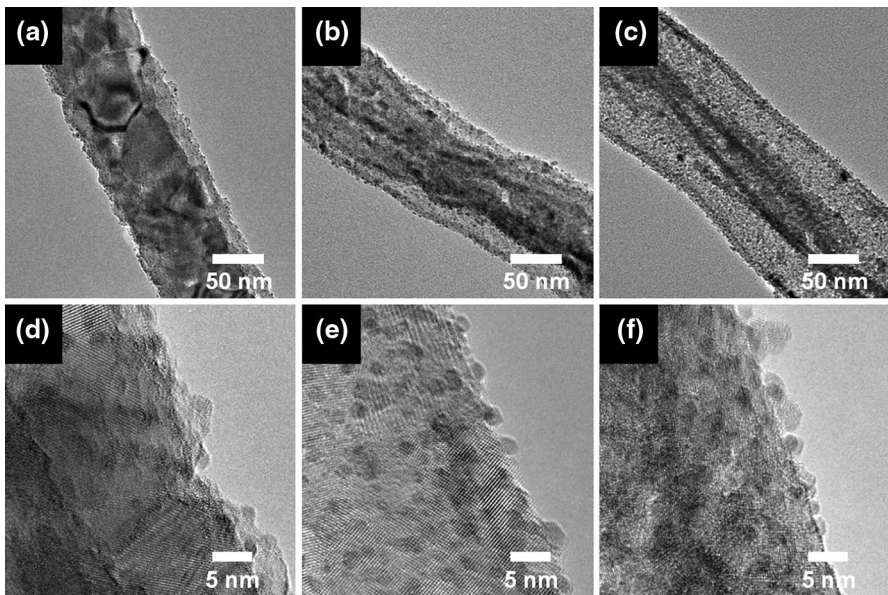**Fig. 1** FESEM images **a–c** obtained from samples *A*, *B*, and *C*

Fig. 2 Low-resolution TEM images (**a–c**) and enlarged TEM images (**d–f**) of samples *A*, *B*, and *C*

respectively, with a spin–orbit splitting of 2.7 eV, corresponding to the Nb_2O_5 phases [17]. The Ti $2p_{3/2}$ and Ti $2p_{1/2}$ spectral peaks exhibit two peaks at ~ 458.4 and ~ 463.5 eV, respectively. This indicates that the Ti element in TiO_2 NFs exists as Ti^{4+} [18]. Thus, the NTO NFs are composed of Nb_2O_5 and TiO_2 phases. Regarding the chemical states of the Ru electrodes, Fig. 4c presents the XPS spectra for the Ru $3d_{5/2}$ and Ru $3d_{3/2}$ photoelectrons. In particular for the Ru $3d_{5/2}$ photoelectrons, two signals are observed at ~ 279.8 and ~ 280.9 eV, corresponding to the metallic Ru nanophase and the RuO_2 nanophase, respectively [19]. These results imply that a metallic Ru nanophase and an oxidized Ru nanophase co-exist because Ru nanophases tend to be easily oxidized when dried at 100 °C [20]. Furthermore, the co-existence of such nanophase Ru–RuO_2 composites would directly affect the performance improvement for electrochemical capacitors.

Fig. 3 XRD plots obtained from samples *A*, *B*, and *C*. The reference bulk reflections of pure RuO$_2$, pure Ru, anatase TiO$_2$, and rutile TiO$_2$ phases are shown at the *bottom*
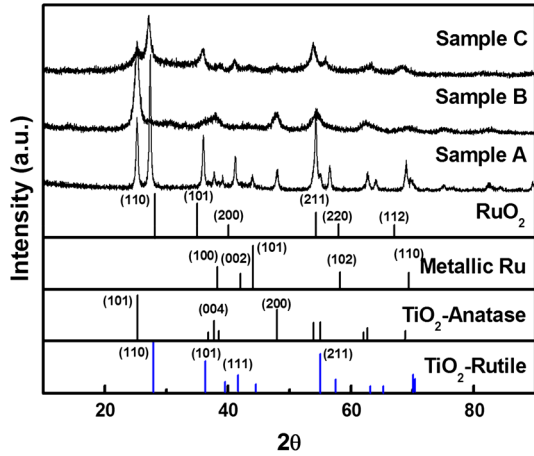

Figure 5a–c shows cyclic voltammograms (CVs) of samples A, B, and C, respectively, which were dried at 100 °C and measured at scan rates of 5, 10, 30, 50, and 100 mV/s in a potential range of 0.0–1.0 V (vs. Ag/AgCl) in a 0.5 M H$_2$SO$_4$ electrolyte. All the samples displayed pseudocapacitance behaviour having faradaic redox reactions. Furthermore, the CVs measured at 5 mV/s (Fig. 5d) clearly exhibited a pseudocapacitance behavior, which indicates that the redox peaks of the samples appeared at 0.4–0.6 V. The reversible electron transfer processes in a pseudocapacitor can be explained using the following reaction [21–23]:

$$RuO_2 + \delta H^+ + \delta e = RuO_{2-\delta}(OH)_\delta (0 \leq \delta \leq 2)$$

The capacitances calculated by considering the weight of the nanophase Ru–RuO$_2$ composites for samples A, B, and C were ∼243.7, ∼304.3, and ∼496.3 F/g, respectively, at a scan rate of 5 mV/s. That is, sample C exhibited excellent capacitance performance as compared to the other samples. In addition, the capacitance of sample C (∼456.8 F/g at 10 mV/s) was 7.8 times higher than that of single RuO$_2$ NFs (∼58.0 F/g at 10 mV/s) as previously reported [24]. Moreover, the initial capacitance of sample C, at a scan rate of 5 mV/s, is approximately 2.03 times higher than that of sample A. This enhancement can be explained by the improved surface area of the NTO NF supports (∼128.4 m^2/g), which allows for a uniform distribution of nanophase Ru–RuO$_2$ composites. It is also explained by the presence of nanophase Ru–RuO$_2$ composites, which was confirmed by XPS measurements. That is, the use of nanophase Ru–RuO$_2$ composites may be related to the improved electrical conductivity of the electrode because of the presence of a metallic Ru nanophase. Therefore, the performance improvement of sample C can be attributed to the wrinkled NTO NF supports having a high surface area and the presence of nanophase Ru–RuO$_2$ composites. Figure 5e presents the capacitances evaluated from Fig. 5a–c as a function of the potential scan rate. Samples A, B, and C exhibited capacitances of ∼178.5, ∼225.8, and ∼264.9 F/g, respectively, at a scan rate of 100 mV/s. Despite the slight reductions in the capacitances up to a scan rate of 100 mV/s, sample C with the wrinkled structure maintained good
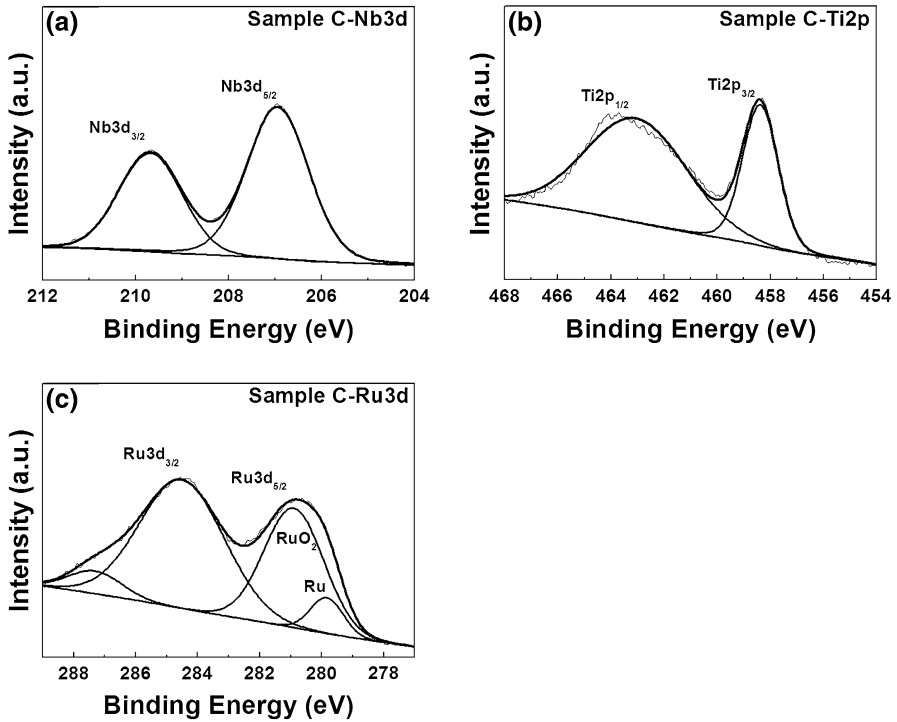
Fig. 4 XPS spectra of **a** Nb 3*d*, **b** Ti 2*p*, and **c** Ru 3*d* core-levels obtained from sample *C*
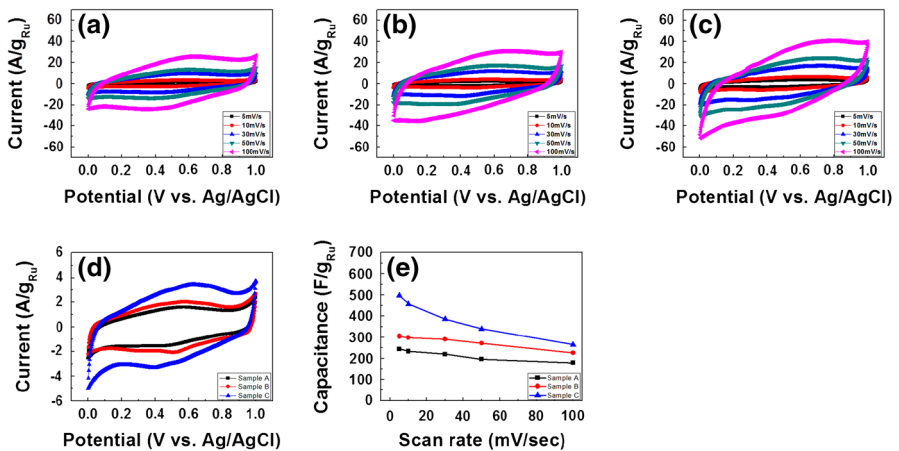

Fig. 5 Cyclic voltammograms (**a–c**) obtained from samples *A*, *B*, and *C* measured at scan rates of 5, 10, 30, 50, and 100 mV/s in the range of 0.0–1.0 V. Cyclic voltammograms (**d**) of the samples measured at a scan rate of 5 mV/s. Capacitances (**e**) evaluated from (**a–c**) as a function of the potential scan rate

capacitance for high-performance electrochemical capacitors. Thus, the nanophase Ru–RuO$_2$ composites decorating the wrinkled NTO NFs are promising candidates for highly efficient electrochemical capacitors.

Conclusions

Nanophase Ru–RuO$_2$ composites decorated on wrinkled NTO NFs were fabricated by electrospinning and impregnation methods. The structure, morphology, and chemical composition of these nanophase composites were investigated using FESEM, TEM, BET, XRD, and XPS measurements. The CV results indicated that sample C exhibited superior capacitance ($\sim$496.3 F/g at 5 mV/s) and good high-rate capacitance because of the synergistic effect of the high surface area of the wrinkled NTO NF supports ($\sim$128.4 m^2/g) and the presence of the nanophase Ru–RuO$_2$ composites.

References

1. P.J. Hall, M. Mirzaeian, S.I. Fletcher, F.B. Sillars, A.J.R. Rennie, G.O. Shitta-Bey, G. Wilson, A. Cruden, R. Carter, Energy Environ. Sci. **3**, 1238 (2010)
2. R. Kötz, M. Carlen, Electrochimi. Acta **45**, 2483 (2000)
3. Y. Zhang, H. Feng, X. Wu, L. Wang, A. Zhang, T. Xia, H. Dong, X. Li, L. Zhang, Int. J. Hydrogen Energy **34**, 4889 (2009)
4. G.H. An, H.J. Ahn, Carbon **65**, 87 (2013)
5. K. Krishnamoorthy, G. Kumar, Veerasubramani, S. Radhakrishnan, S.J. Kim, Mater. Res. Bull. **50**, 499 (2014)
6. H. Pang, S. Wang, W. Shao, S. Zhao, B. Yan, X. Li, S. Li, J. Chen, W. Du, Nanoscale. **5**, 5752 (2013)
7. G. Yu, X. Xie, L. Pan, Z. Bao, Y. Cui, Nano Energy **2**, 213 (2013)
8. X.M. Liu, X.G. Zhang, Electrochimi. Acta **49**, 229 (2004)
9. G.H. An, H.J. Ahn, Electrochem. Solid-State Lett. **2**, M33 (2013)
10. L.M. Huang, H.Z. Lin, T.C. Wen, A. Gopalan, Electrochimi. Acta **52**, 1058 (2006)
11. S.L. Gojkovic′, B.M. Babic′, V.R. Radmilovic′, N.V. Krstajic′, J. Electroanal. Chem. **639**, 161 (2010)
12. Y. Wang, B.M. Smarsly, I. Djerdj, Chem. Mater. **22**, 6624 (2010)
13. M.A. Gillispie, M.F.A.M. van Hest, M.S. Dabney, J.D. Perkins, D.S. Ginley, J. Mater. Res. **22**, 2832 (2007)
14. H.L. An, H.J. Ahn, Mater. Lett. **93**, 88 (2013)
15. H.J. Ahn, Y.E. Sung, W.B. Kim, T.Y. Seong, Electrochem. Solid-State Lett. **11**, A112 (2008)
16. C.L. Pai, M.C. Boyce, G.C. Rutledge, Macromolecules **42**, 2102 (2009)
17. M.Z. Atashbar, H.T. Sun, B. Gong, W. Wlodarski, R. Lamb, Thin Solid Films **326**, 238 (1998)
18. S.I. Noh, D.W. Park, H.S. Shim, H.J. Ahn, J. Nanosci. Nanotechnol. **12**, 6065 (2012)
19. R. Kotz, H.J. Lewerenz, S. Stucki, J. Electrochem. Soc. **130**, 825 (1983)
20. W. Chen, M. Zhang, D.W. Zhang, S.J. Ding, J.J. Tan, M. Xu, X.P. Qu, L.K. Wang, Appl. Surf. Sci. **253**, 4045 (2007)
21. G.H. Deng, X. Xiao, J.H. Chen, X.B. Zeng, D.L. He, Y.F. Kuang, Carbon **43**, 1557 (2005)
22. L. Mayrand-Provencher, D. Rochefort, J. Phys. Chem. C **113**, 1632 (2009)
23. C.Y. Lee, A.M. Bond, Langmuir **26**, 16155 (2010)
24. J.B. Lee, S.Y. Jeong, W.J. Moon, T.Y. Seong, H.J. Ahn, J. Alloys Compd. **509**, 4336 (2011)